OPEN ACCESS

University of BRISTOL

Bzdek, B., & Walker, J. (2019). Vibrational Spectroscopy of Individual Aerosol Droplets by Optical Tweezers. *Spectroscopy*, *34*(4), 22-31.

Peer reviewed version

Link to publication record in Explore Bristol Research
PDF-document

University of Bristol - Explore Bristol Research

General rights

Vibrational Spectroscopy of Individual Aerosol Droplets by Optical Tweezers

Bryan R. Bzdek[1,] and Jim S. Walker[1,2]*

[1]School of Chemistry, University of Bristol, Cantock's Close, Bristol, BS8 1TS, United Kingdom

[2]Bristol Industrial and Research Associates Ltd (Biral), Unit 8 Harbour Road Trading Estate, Portishead, Bristol BS20 7BL, United Kingdom

Submitted to:

Spectroscopy

*To whom correspondence should be addressed. Electronic mail: b.bzdek@bristol.ac.uk. Phone: +44 (0)117 331 8387

ABSTRACT

Aerosols are key components in a wide range of environmental systems and industrial contexts spanning air pollution and clouds to engineered nanomaterials to drug delivery to the lungs. However, the basic properties of aerosols are often elusive due to their small sizes and capacity to rapidly respond to changing ambient conditions. In this instalment of Molecular Spectroscopy Workbench, we discuss Raman spectroscopy of individual picolitre volume droplets using optical tweezers. Single droplet spectroscopy enables highly accurate and precise measurements of droplet size and refractive index, as well as measurement of droplet chemical composition. Time-resolved measurements permit investigation of fundamental droplet properties including hygroscopic response, vapour pressure, and surface and bulk characteristics. Such information improves our molecular level understanding of chemical processes within single droplets and facilitates broader understanding of complex systems.

INTRODUCTION

Aerosols, which are solid particles or liquid droplets suspended in air, are ubiquitous. Aerosols negatively affect human health through air pollution,[1] but also improve health by serving as delivery agents for pharmaceutics.[2] With respect to the atmosphere, aerosols are generally thought to cool climate by scattering solar radiation and by serving as the seeds for cloud droplets.[3] Aerosols also have a wide range of industrial applications, including spray drying, inkjet printing, personal care products, combustion, and agricultural chemicals. To resolve aerosol impacts on health and climate, or to engineer effective industrial products, knowledge of properties like particle size, composition, interaction with light, and surface and bulk properties is required. Moreover, it is beneficial to resolve these properties on a single particle basis, as even a nominally homogeneous and monodisperse particle ensemble has inherent distributions in key properties like particle size.

Aerosols are intrinsically interesting because they exhibit unique properties relative to bulk systems.[4] Figure 1 highlights some of these interesting properties with a hygroscopic growth curve for a sodium chloride (NaCl) particle, plotting a change in droplet mass (relative to a dry particle) against ambient relative humidity (RH). At low RH, NaCl aerosol contains no water and is therefore a solid particle. With increasing RH, water adsorbs to the solid particle surface until reaching the deliquescence RH (~75% for NaCl), which is the RH at which the solid particle absorbs enough water to undergo spontaneously a phase transition to a liquid droplet and is equivalent to the water activity at the solubility limit of a bulk solution of NaCl. Beyond this point, the liquid droplet size increases with increasing RH. Starting from a liquid droplet at high RH, lowering RH decreases droplet size due to water evaporation. However, rather than undergo a phase change at the deliquescence RH, the droplet will continue to shrink until reaching the efflorescence RH (~43% RH for NaCl), which is the RH where the liquid droplet spontaneously undergoes a phase change to form a solid particle and highlights a hysteresis in phase that depends on the direction of the RH change. This observation is remarkable: liquid droplets between the deliquescence and efflorescence RH can exist in metastable, supersaturated solute states. In the case of NaCl, the aqueous concentration at the deliquescence RH (i.e. the bulk solubility limit) is 6.2 molal, whereas at the efflorescence RH it is 13.2 molal. For a soluble organic the solute concentration can range from ~5 molal at the deliquescence RH to >30 molal at dry conditions. Such compositions can exhibit highly non-ideal behaviour and may inhibit nucleation of a solid particle, instead forming an amorphous glass. The high surface to volume ratio of aerosols also means that particles can respond rapidly

71 (<1 ms) to changes in the gas phase, potentially resulting in different product distributions after

72 a reaction due to size-dependent competition among gas-diffusion, surface accommodation,

73 and particle bulk transport.

74   To measure individual droplet properties by spectroscopic approaches, the droplet

75 location must first be controllable. Optical tweezers are one method to capture and manipulate

76 3-10 μm radius droplets over long time periods. The approach, recently recognised by the 2018

77 Nobel Prize awarded to Arthur Ashkin, employs a tightly focussed laser beam to create a

78 gradient force optical trap that immobilises a particle by exploiting the refractive index (RI)

79 difference between the particle and surrounding medium. Optical tweezers are perhaps better

80 known for applications to condensed systems, but in fact some of the early optical trapping

81 work captured liquid droplets in air.[5,6] Figure 2 illustrates a typical aerosol optical tweezers

82 (AOT) setup, similar to that sold commercially by Biral, configured to allow production of

83 multiple, steerable optical traps for the study of droplet coalescence.[7,8] A spatial light modulator

84 dynamically shapes the phase front of a continuous wave 532 nm laser to form multiple,

85 steerable optical traps. When the trap separation is sufficiently small, droplet coalescence is

86 induced. Brightfield imaging is accomplished by a blue LED. Backscattered Raman light is

87 imaged onto the entrance slit of a spectrograph to perform single droplet spectroscopy. Elastic

88 backscattered light, the intensity of which varies during droplet coalescence, is directed to a

89 photodiode and recorded with an oscilloscope. Droplets are typically nebulised from solution

90 and captured in an isolated RH-controlled trapping chamber. This approach enables

91 measurement of a range of physical and chemical properties of an optically trapped droplet.

92   In this article, we describe the utility of the AOT approach to characterise

93 spectroscopically individual picolitre volume droplets. We first discuss the principles of cavity

94 enhanced Raman spectroscopy and then highlight the precise and time-resolved measurements

95 of chemical and physical properties enabled by these measurements.

96

97 **RAMAN SPECTROSCOPY OF INDIVIDUAL DROPLETS**

98   Cavity enhanced Raman spectroscopy is the primary tool for analysing optically

99 tweezed droplets because it allows high precision measurements of size and RI, as well as

100 information about droplet chemical composition. The AOT setup permits efficient acquisition

101 of Raman scattered light because the trapping laser beam and microscope objective are also

102 used as a Raman excitation source and high efficiency collection optic, respectively, allowing

103 a time resolution <1 s.

104   Figure 3a shows a Raman spectrum from an optically tweezed aqueous sucrose droplet.

105 The Raman signal consists of two components: the spontaneous signal and the stimulated

106 signal.[9–14] The spontaneous signal is the broad, underlying Stokes band that provides

107 information about the droplet's chemical composition. The stimulated signal presents as the

108 superimposed structure and arises because the spherical droplet behaves as a low loss optical

109 cavity at wavelengths commensurate with whispering gallery modes (WGMs). When

110 spontaneous Raman emission overlaps with a WGM, a standing wave forms around the

111 circumference of the droplet and stimulates further emission at the same frequency, resulting

112 in sharp peaks at discrete wavelengths. Each stimulated peak is described by a mode order n

113 (defined by the number of standing waves around the droplet circumference) and mode number

114 l (defined by the number of radial maxima in the distribution of the mode intensity). For each

115 mode number and mode order, there exists a transverse electric (TE) mode (having no radial

116 electric field component) and a transverse magnetic (TM) mode (having no radial magnetic

117 field).

118   WGM wavelengths are highly sensitive to droplet size and composition. Figure 3b

119 illustrates the magnitude of the shifts in WGM wavelengths as an aqueous sucrose droplet

120 changes radius in response to a change in ambient RH. WGM wavelengths can be calculated

121 using Mie theory[15] if the size and RI are known. The wavelengths at which stimulated Raman

122 signals are observed experimentally are compared to a library of Mie theory simulations

123 calculated for various size and RI combinations, with the best match giving the correct size and

124 RI. The comparison can be performed in <1 s using custom built software, allowing the

125 physical properties of the droplet to be tracked in real time with accuracy of ±2 nm in radius

126 and 0.0005 in RI.[16] The next sections illustrate how such accurate and precise measurements

127 permit elucidation of a wide range of fundamental droplet properties.

128

129 **HYGROSCOPICITY AND VAPOUR PRESSURE**

130   Figure 4 shows a change in the properties of a glycerol droplet as RH is systematically

131 decreased. These data were collected using the commercially available instrument from Biral.

132 Small changes in WGM wavelengths can be related to precise changes in droplet radius (Fig.

133 4a) and RI (Fig. 4b). As RH is stepped from 80% to 30% in 10% intervals, the droplet responds

134 by losing water, resulting in a step change in droplet size. This loss of water also increases the

135 glycerol concentration, leading to a corresponding increase in droplet RI, as the RI of glycerol

136 is larger than that of water. Note the high precision in the measurement, indicating very little

137 second-to-second variation in droplet parameters. The observed changes in droplet size and RI

describe the hygroscopic response of the droplet. Hygroscopicity impacts the number and size distribution of atmospheric cloud droplets, as well as the optical properties of atmospheric aerosol. Because particle deposition in the respiratory tract is size-dependent, hygroscopicity also influences deposition and ultimately health effects.

Figure 5 shows how hygroscopic response can be used to identify changes in particle composition.[17] Figure 5a-b shows droplet radius and RI (retrieved from the stimulated Raman signal), whereas Fig. 5c shows the ratio of the intensities of the C-H to O-H stretching regions in the spontaneous Raman signal ($I\nu_{C-H}/I\nu_{O-H}$). Initially, a NaCl droplet is captured and equilibrated to a constant gas flow at 80% RH. During 1000-1400 s, a flow of aqueous NaCl aerosol is introduced into the trapping chamber without altering the ambient RH. The introduced aqueous droplets coalesce with the trapped droplet, increasing the trapped droplet's radius but maintaining the same RI, as the droplet chemical composition remains unchanged. Then, during 3000-3400 s, a flow of aqueous sucrose aerosol is introduced into the trapping chamber, again maintaining an RH around 80%. In this case, droplet size changes due to the accretion of sucrose aerosol. The accretion of sucrose also increases the droplet RI, and the resulting change in droplet composition is reflected in the observed increase in the $I\nu_{C-H}/I\nu_{O-H}$ ratio.

The changes in radius and RI can be visualised in a plot of radial growth factor (GF_d) against droplet RI or RH. Any droplet will have a well-defined relationship between real RI and RH owing to the relationship between RI and solute concentration, provided the droplet chemical composition does not change beyond water uptake or loss in response to changes in ambient RH. This relationship leads to a defined trajectory between droplet RI and droplet wet radius (r_{wet}). However, dry particle radius, r_{dry}, will vary from measurement to measurement. A plot of radial growth factor [GF_d (RH)] accounts for variations in particle dry size by defining the change in r_{wet} relative to r_{dry}:

$$GF_d(RH) = \frac{r_{wet}}{r_{dry}} \qquad (1)$$

Figure 5d shows a plot of GF_d against RI for three NaCl droplets (black, blue, and red symbols) studied across a wide range in RH (96% to 49% RH, corresponding to refractive indices of 1.345 to 1.410, respectively). All these data collapse onto each other (visually represented by the line), illustrating the reproducibility in hygroscopic growth afforded by the AOT approach across multiple measurements. The green symbols show the hygroscopic growth of the NaCl droplet doped with sucrose aerosol (i.e. $t > \sim 3400$ s in Fig. 5a-c). The offset is due to the change in the relationship between droplet composition and equilibrium size as

171   RH is varied and highlights how compositional changes that result in only a few percent change

172   in droplet radius can be resolved due to the high accuracy of droplet size and RI obtained from

173   the Raman signal.

174   Although droplet size may change substantially due to changes in the RH around the

175   droplet, size may also change due to evaporation of semivolatile molecules from the droplet.[18]

176   This evaporation is evident in Fig. 4, as in between the step changes in droplet size due to RH

177   steps, the glycerol droplet size decreases linearly and its RI increases linearly (dotted lines)

178   owing to its vapour pressure ($p^0_G \approx 10^{-2}$ Pa). A molecule's vapour pressure is fundamentally

179   important because it determines partitioning between the gas and condensed phases. The slower

180   change in droplet size and RI is due to the evaporation of glycerol (as well as commensurate

181   water to maintain the droplet water activity equivalent to the RH). In the experiment, a

182   humidified N_2 flow is used, resulting in a concentration gradient from the droplet surface to the

183   gas phase, leading to slow volatilisation of glycerol at a rate governed by its vapour pressure

184   at the solution composition, p_G, which in turn depends on the glycerol mole fraction, x_G, and

185   the activity coefficient, γ_G:

186   $$p_G = x_G \gamma_G p_G^0 \qquad (2)$$

187   Measurement of the rate of change in droplet size (dr^2/dt) is related to p^0 for a given molecule

188   through the Maxwell equation:

189   $$\frac{dr^2}{dt} = \frac{2M_i D_{i,air}}{RT\rho F_i}\left(p_{i,\infty} - p_{i,r}\right) \quad (3)$$

190   where M_i is the molecular mass of semivolatile compound i, D_i is its diffusion constant in the

191   surrounding gas, R is the ideal gas constant, T is temperature, ρ is droplet density, F_i is the mass

192   fraction of compound i, $p_{i,r}$ is the vapour pressure in equilibrium at the droplet surface, and $p_{i,\infty}$

193   is partial pressure of the molecule at infinite distance from the droplet surface (assumed zero).

194

195   **AEROSOL SURFACE AND BULK PROPERTIES**

196   We next discuss droplet surface and bulk properties, which are key to a range of

197   processes. For example, surface tension helps determine what fraction of atmospheric particles

198   grow into cloud droplets by governing the critical supersaturation in RH that must be

199   surpassed.[19] Moreover, the surface composition of droplets can affect the transport of

200   molecules like water into and out of the droplet[20] as well as promote very different reactions

201   from those occurring in the droplet bulk.[21] Knowledge of bulk properties allows a better

202   understanding of transport processes within the droplet, which can help explain droplet

203   heterogeneity, reactivity, and composition.[22] For example, a highly viscous droplet can inhibit

204 diffusion of reactant molecules, resulting in slower apparent reaction rates.[23] Understanding

205 the interplay between surface and bulk properties enables control over droplet structure, which

206 is important in many industrial contexts.[24]

207   Surface and bulk droplet properties can be investigated by coalescence of two droplets.

208 Droplets are captured in individual traps, equilibrated to a desired ambient condition, and then

209 brought into coalescence at a user-defined time. For low viscosity droplets, coalescence

210 proceeds through damped oscillations in droplet shape. Figure 6a shows high frame rate images

211 of a dilute NaCl droplet coated with surfactant immediately after coalescence.[8] Although high

212 frame rate imaging visualises the coalescence dynamics, it is more efficient to resolve the

213 coalescence by collection of elastic backscattered light (see Fig. 2). Figure 6b shows the elastic

214 backscattered light from the coalescence event in Fig. 6a, along with the aspect ratios from the

215 high frame rate images. Surface tension is determined by the equation:[25,26]

216
$$\sigma = \frac{\omega_l^2 a^3 \rho}{l(l-1)(l+2)} \qquad (4)$$

217 where σ is surface tension, ω_l is the oscillation frequency for mode l (corresponding to a

218 characteristic deformation in droplet shape), a is droplet radius, and ρ is droplet density. Note

219 that accurate measurement of surface tension depends on a precise measurement of droplet

220 radius (a^3 term), highlighting the benefits afforded by size characterisation using the stimulated

221 Raman spectrum. The Fast Fourier Transform of the elastic backscattered light signal allows

222 retrieval of ω_l (Fig. 6c). It is then straightforward to calculate the droplet surface tension. Figure

223 6d shows surface tensions retrieved using a holographic AOT setup for droplets containing

224 NaCl, glutaric acid, and a 1:1 mass mixture of both solutes. These measurements compare

225 favourably to a statistical thermodynamic model.[27] Moreover, a key benefit of performing the

226 surface tension measurement on droplets is the ability to access supersaturated solute states

227 that are inaccessible to bulk approaches. The measured values to the right of the vertical lines

228 in Fig. 6d are in the supersaturated solute regime and demonstrate the benefit of aerosol

229 measurements to test models in previously untestable regimes. In addition, measurements have

230 highlighted that trace contaminants in air rapidly lower the surface tension of droplets to values

231 consistent with those of surfactant solutions.[8]

232   If the droplet viscosity is above a critical value, the surface oscillations are

233 instantaneously damped and coalescence proceeds through a slow merging of two droplets.[7,28]

234 This concept is demonstrated in Fig. 7a with images of coalescing sucrose droplets that have

235 been equilibrated to different RH values.[29] Figure 7b shows that aspect ratios of the slowly

236 coalescing droplets follow an exponential decay, and that depending on the droplet viscosity

237 (governed by RH), the relaxation timescale (τ_l) can span from microseconds to days. The

238 relaxation timescale is related to droplet viscosity by the equation:

239 $$\eta = \frac{l(l+2)(2l+1)}{2(2l^2+4l+3)}\frac{\sigma\tau_l}{a} \approx \frac{\sigma\tau_{l=2}}{a} \qquad (5)$$

240 where η is the droplet viscosity.

241 Figure 7c shows viscosity measurements of citric acid by both bulk and AOT

242 approaches, comparing to 1,4-butanetriol and sucrose over the entire range of RH. This figure

243 highlights the utility of the AOT approach to measuring viscosity. First, measurements can be

244 made over a wide range of viscosities, from values similar to that of pure water (1 mPa·s) to

245 values beyond the glass transition (10^{10} Pa·s), spanning >13 orders of magnitude. Moreover,

246 because it is straightforward to produce droplets containing highly viscous, supersaturated

247 solute states, this approach can measure material properties under conditions inaccessible in

248 bulk systems. For example, bulk solutions of citric acid can only reach concentrations

249 corresponding to water activities ~0.8 (80% RH), the bulk solubility limit. However, in the

250 aerosol phase the solubility limit is easily exceeded, and measurements of viscous citric acid

251 droplets are possible across the entire range of water activity, with viscosity values extending

252 more than six orders of magnitude larger than those accessible in bulk solution, permitting

253 comparison to model predictions and allowing estimation of the viscosity of atmospheric

254 particles.[28]

255

256 **PUTTING IT ALL TOGETHER**

257 The previous sections highlight fundamental measurements possible due to single

258 droplet Raman spectroscopy. We now present an example where spectroscopy was used to

259 evaluate how changes in viscosity impact the droplet's reactivity with ozone, a common

260 atmospheric oxidant.[30] In the experiment, a droplet containing the semivolatile compound

261 maleic acid (vapour pressure ~10^{-3} Pa), non-volatile sucrose, and water was equilibrated to

262 different RH values. As discussed earlier, when a droplet containing a semivolatile compound

263 is held at constant RH, its size will slowly decrease due to evaporation of the semivolatile

264 compound and an appropriate amount of solvating water. From the size change (inferred from

265 the changes to stimulated Raman band positions), the compound's pure component vapour

266 pressure is inferred from Eq. 3. Figure 8a illustrates the time-dependent fractional change in

267 size for a droplet containing 5:1 maleic acid:sucrose held at different RH values. At higher RH

268 (e.g. 70%) a steeper gradient in the radius change is observed as opposed to when the droplet

269 is held at a much lower RH (e.g. 10%). However, based purely on vapour pressure

270 considerations, the mass flux of maleic acid is expected to increase with decreasing RH, as the

271 maleic acid mole fraction is increased at low RH. In fact, when the effective vapour pressure

272 is calculated using Eq. 3, the retrieved values span from $<10^{-5}$ Pa at 10% to 10^{-3} Pa (the true

273 value) at 70% RH. The reason for this observation is kinetic suppression of the evaporation

274 rate. The non-volatile sucrose component increases droplet viscosity, consequently inhibiting

275 diffusion of maleic acid within the particle. The decreased diffusion constant makes it harder

276 for maleic acid to reach the droplet surface and evaporate.

277 Figure 8b shows relative changes in the intensity of the vinylic C-H stretch in the

278 spontaneous Raman spectrum when maleic acid-sucrose droplets held at different RH values

279 are exposed to the oxidant ozone. Ozone reacts with maleic acid (which contains a carbon-

280 carbon double bond) but not with sucrose (which lacks a C=C bond). Ozonolysis fragments

281 maleic acid at the double bond, forming lower molecular weight molecules with a range of

282 vapour pressures. Monitoring the vinylic C-H stretch provides a direct measure of the reaction

283 rate of maleic acid through cleavage of the carbon-carbon double bond. There is a clear RH

284 dependence for reactivity (Fig. 8b), with droplets at higher RH exhibiting faster reaction

285 kinetics. For comparison, the purple triangles show the change in $I_{\nu C\text{-}H}$ for a maleic acid droplet

286 held at 73% RH in the absence of ozone (i.e. change in signal intensity entirely due to

287 evaporation of semivolatile maleic acid). The golden triangles show reaction of a 10:1

288 sucrose:maleic acid mixture at 40% RH, demonstrating that ozonolysis is effectively shut

289 down. From the spontaneous Raman data, reaction probabilities for ozone uptake can be

290 estimated. For the 5:1 sucrose:maleic acid droplet at 75% RH, the reaction probability is similar

291 to that retrieved from an experiment in the bulk ($\sim 8 \times 10^{-6}$). However, for the 10:1

292 sucrose:maleic acid droplet at 40% RH, the reaction probability decreases by more than two

293 orders of magnitude to $<3 \times 10^{-8}$. The explanation for the lowering of the uptake coefficient is

294 the change in diffusivity for water and ozone that results from the matrix formed by interactions

295 of sucrose and maleic acid.

296 This example demonstrates how precise measurement of changes to droplet size can

297 provide information about the phase state of a droplet, permitting insight on diffusion within

298 the droplet. Coupling those observations with spontaneous Raman spectra allows

299 rationalisation of the reactivity of droplets as a function of their viscosity.

300

301 **CONCLUSIONS**

302   Aerosols are complex, highly non-ideal systems that exhibit properties that often cannot
303 easily be represented by bulk studies. Optical tweezers are a versatile approach to study
304 problems in aerosol science on a single droplet level, with a wide range of potential applications
305 spanning atmospheric science to materials science and pharmaceuticals. We showed that single
306 droplet Raman spectroscopy provides a spontaneous Raman signal that gives information on
307 chemical composition and a stimulated Raman signal when the spherical droplet behaves as a
308 low loss optical cavity at wavelengths commensurate with WGMs. Because WGM
309 wavelengths are highly sensitive to droplet size and composition, comparison of experimental
310 resonances to those predicted by Mie theory permits accurate and precise retrieval of the
311 droplet's size and RI (to ±2 nm and 0.0005, respectively). Consequently, dynamic changes to
312 droplet physical, chemical, and optical properties can be monitored with high time resolution.
313 These changes to droplet properties enable determination of fundamental droplet properties
314 including hygroscopic response, vapour pressure, surface tension, and bulk viscosity. Such
315 information allows insight into molecular processes occurring within picolitre volumes,
316 including how parameters like viscosity can affect the volatilisation and reactivity of
317 semivolatile compounds in the droplet. Because aerosol science is fundamental to many
318 research areas, the AOT approach has broad utility.

319

REFERENCES

1. Lelieveld, J.; Evans, J. S.; Fnais, M.; Giannadaki, D.; Pozzer, A. *Nature* **525**, 367–371, (2015).
2. Forbes, B.; Asgharian, B.; Dailey, L. A.; Ferguson, D.; Gerde, P.; Gumbleton, M.; Gustavsson, L.; Hardy, C.; Hassall, D.; Jones, R.; Lock, R.; Maas, J.; McGovern, T.; Pitcairn, G. R.; Somers, G.; Wolff, R. K. *Adv. Drug Deliv. Rev.* **63**, 69–87, (2011).
3. IPCC. Stocker, T. F., Qin, D., Plattner, G.-K., Tignor, M., Allen, S. K., Boschung, J., Nauels, A., Xia, Y., Bex, V., Midgley, P. M., Eds.; Cambridge University Press: Cambridge.
4. Bzdek, B. R.; Reid, J. P. *J. Chem. Phys.* **147**, 220901, (2017).
5. Ashkin, A. *Phys. Rev. Lett.* **24**, 156–159, (1970).
6. Ashkin, A.; Dziedzic, J. M. *Science* **187**, 1073–1075, (1975).
7. Power, R. M.; Simpson, S. H.; Reid, J. P.; Hudson, A. J. *Chem. Sci.* **4**, 2597–2604, (2013).
8. Bzdek, B. R.; Power, R. M.; Simpson, S. H.; Reid, J. P.; Royall, C. P. *Chem. Sci.* **7**, 274–285, (2016).
9. Symes, R.; Sayer, R. M.; Reid, J. P. *Phys. Chem. Chem. Phys.* **6**, 474–487, (2004).
10. Ashkin, A.; Dziedzic, J. M. *Phys. Rev. Lett.* **38**, 1351–1354, (1977).
11. Qian, S.-X.; Chang, R. K. *Phys. Rev. Lett.* **56**, 926–929, (1986).
12. Thurn, R.; Kiefer, W. *Appl. Opt.* **24**, 1515, (1985).
13. Vahala, K. J. *Nature* **424**, 839–846, (2003).
14. Trevitt, A. J.; Wearne, P. J.; Bieske, E. J.; Schuder, M. D. *Opt. Lett.* **31**, 2211, (2006).
15. Mie, G. *Ann. Phys.* **25**, 377–445, (1908).
16. Preston, T. C.; Reid, J. P. *J. Opt. Soc. Am. B* **30**, 2113–2122, (2013).
17. Haddrell, A. E.; Miles, R. E. H.; Bzdek, B. R.; Reid, J. P.; Hopkins, R. J.; Walker, J. S. *Anal. Chem.* **89**, 2345–2352, (2017).
18. Pope, F. D.; Tong, H. J.; Dennis-Smither, B. J.; Griffiths, P. T.; Clegg, S. L.; Reid, J. P.; Cox, R. A. *J. Phys. Chem. A* **114**, 10156–10165, (2010).
19. Ovadnevaite, J.; Zuend, A.; Laaksonen, A.; Sanchez, K. J.; Roberts, G.; Ceburnis, D.; Decesari, S.; Rinaldi, M.; Hodas, N.; Facchini, M. C.; Seinfeld, J. H.; O'Dowd, C. *Nature* **546**, 637–641, (2017).
20. Davies, J. F.; Miles, R. E. H.; Haddrell, A. E.; Reid, J. P. *Proc. Natl. Acad. Sci.* **110**, 8807–8812, (2013).
21. Knipping, E. M.; Lakin, M. J.; Foster, K. L.; Jungwirth, P.; Tobias, D. J.; Gerber, R. B.; Dabdub, D.; Finlayson-Pitts, B. J. *Science* **288**, 301–306, (2000).
22. Reid, J. P.; Bertram, A. K.; Topping, D. O.; Laskin, A.; Martin, S. T.; Petters, M. D.; Pope, F. D.; Rovelli, G. *Nat. Commun.* **9**, 956, (2018).
23. Kuwata, M.; Martin, S. T. *Proc. Natl. Acad. Sci.* **109**, 17354–17359, (2012).
24. Baldelli, A.; Vehring, R. *Aerosol Sci. Technol.* **50**, 1130–1142, (2016).
25. Rayleigh, L. *Proc. R. Soc. London* **29**, 71–97, (1879).
26. Chandrasekhar, S. *Proc. London Math. Soc.* **s3-9**, 141–149, (1959).
27. Boyer, H. C.; Bzdek, B. R.; Reid, J. P.; Dutcher, C. S. *J. Phys. Chem. A* **121**, 198–205, (2017).
28. Song, Y. C.; Haddrell, A. E.; Bzdek, B. R.; Reid, J. P.; Bannan, T.; Topping, D. O.; Percival, C.; Cai, C. *J. Phys. Chem. A* **120**, 8123–8137, (2016).
29. Bzdek, B. R.; Collard, L.; Sprittles, J. E.; Hudson, A. J.; Reid, J. P. *J. Chem. Phys.* **145**, 054502, (2016).
30. Marshall, F. H.; Miles, R. E. H.; Song, Y. C.; Ohm, P. B.; Power, R. M.; Reid, J. P.; Dutcher, C. S. *Chem. Sci.* **7**, 1298–1308, (2016).
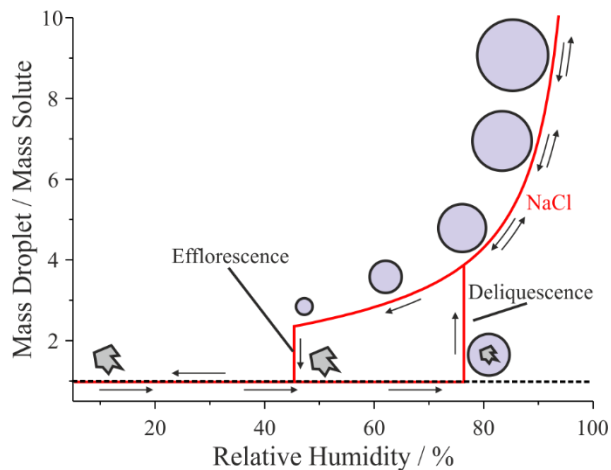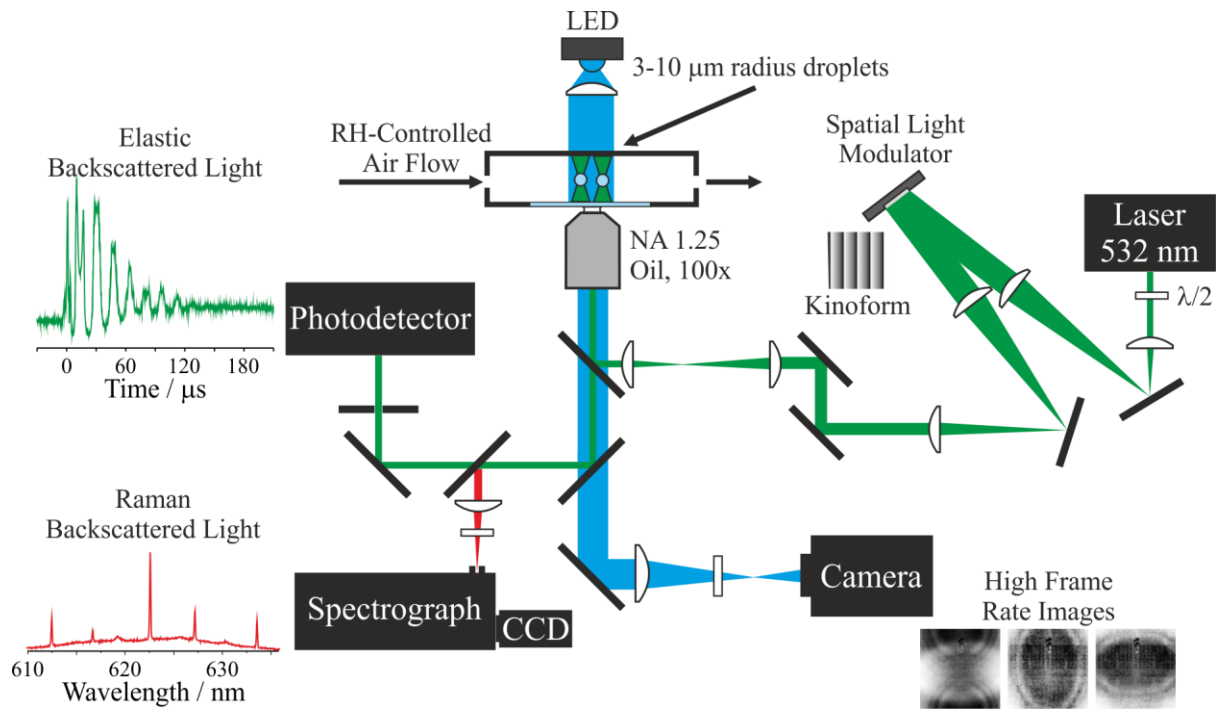
FIGURES

Figure 1: Illustration of a hygroscopic growth curve for a NaCl particle. Note the hysteresis in
particle phase between 43% and 75% RH, where depending on the RH pathway NaCl is either
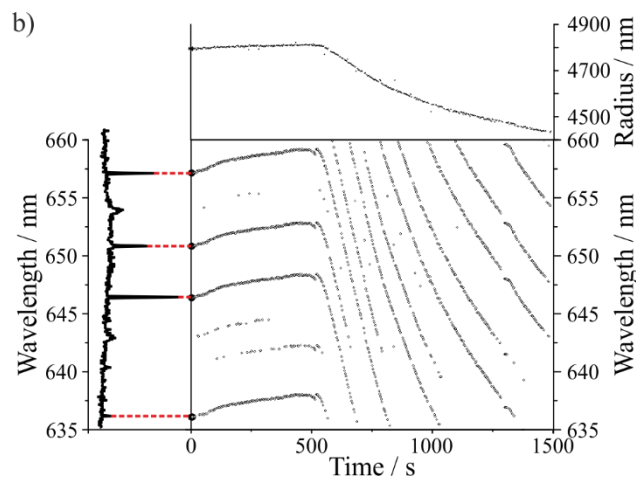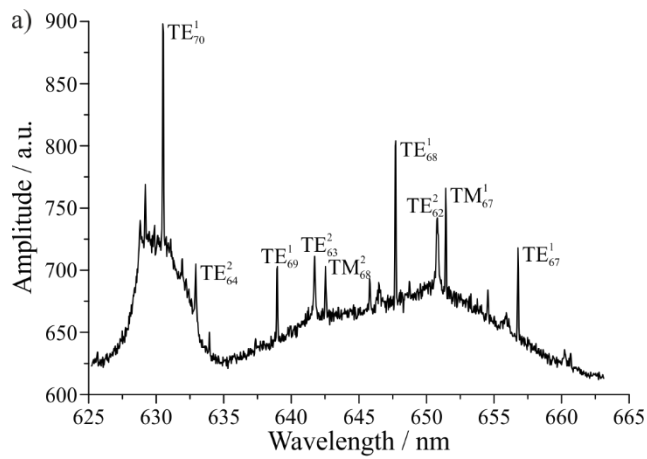a solid particle or a liquid droplet.

378

Figure 2: Schematic of a holographic AOT setup capable of collecting Raman spectra on individual droplets as well as elastic backscattered light to study droplet coalescence.[7,8]

379

380

381

Figure 3: a) A cavity enhanced Raman spectrum of an optically tweezed aqueous sucrose droplet. The spontaneous Raman signal centred around 650 nm is the O-H stretching vibration of water, whereas the signal around 630 nm is the C-H stretching vibration. The stimulated Raman signal is the superimposed structure on the spontaneous band. b) WGM position is closely related to droplet size.

389
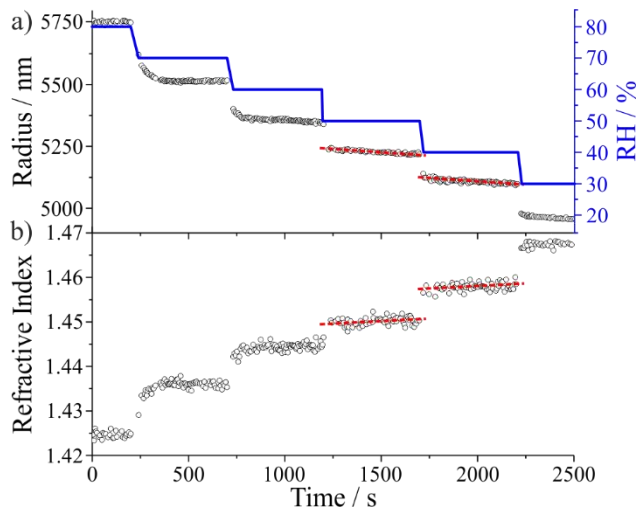
Figure 4: Response of a glycerol droplet to changes in ambient RH. Changes in WGM position
are used to quantify changes in a) droplet radius and b) RI. The red dotted lines indicate the
loss of semivolatile glycerol during periods of constant RH.
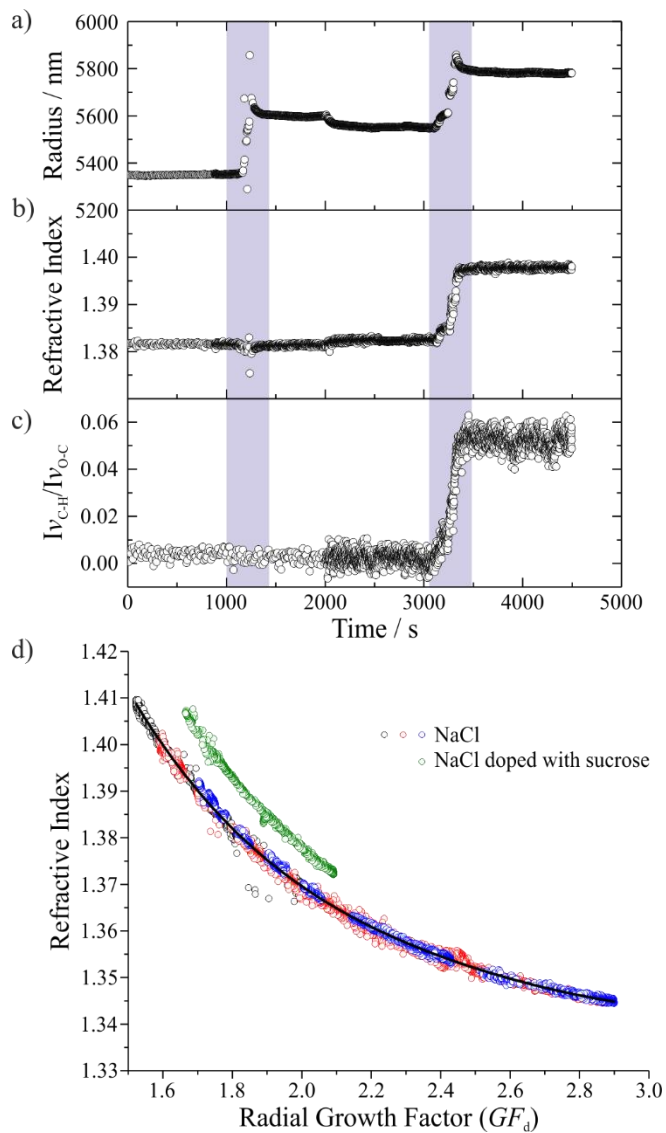
Figure 5: Droplet a) radius, b) RI, and c) chemical composition for a coalescence sampling measurement. In the first coalescence window (first purple box), a flow of aqueous NaCl droplets was introduced. In the second coalescence window, a flow of aqueous sucrose droplets was introduced. d) Comparison of the RI-growth factor (GF_d) relationship for NaCl droplets (black, red, and blue) and a NaCl droplet after a period of coalescence sampling of sucrose aerosol (green).[17]
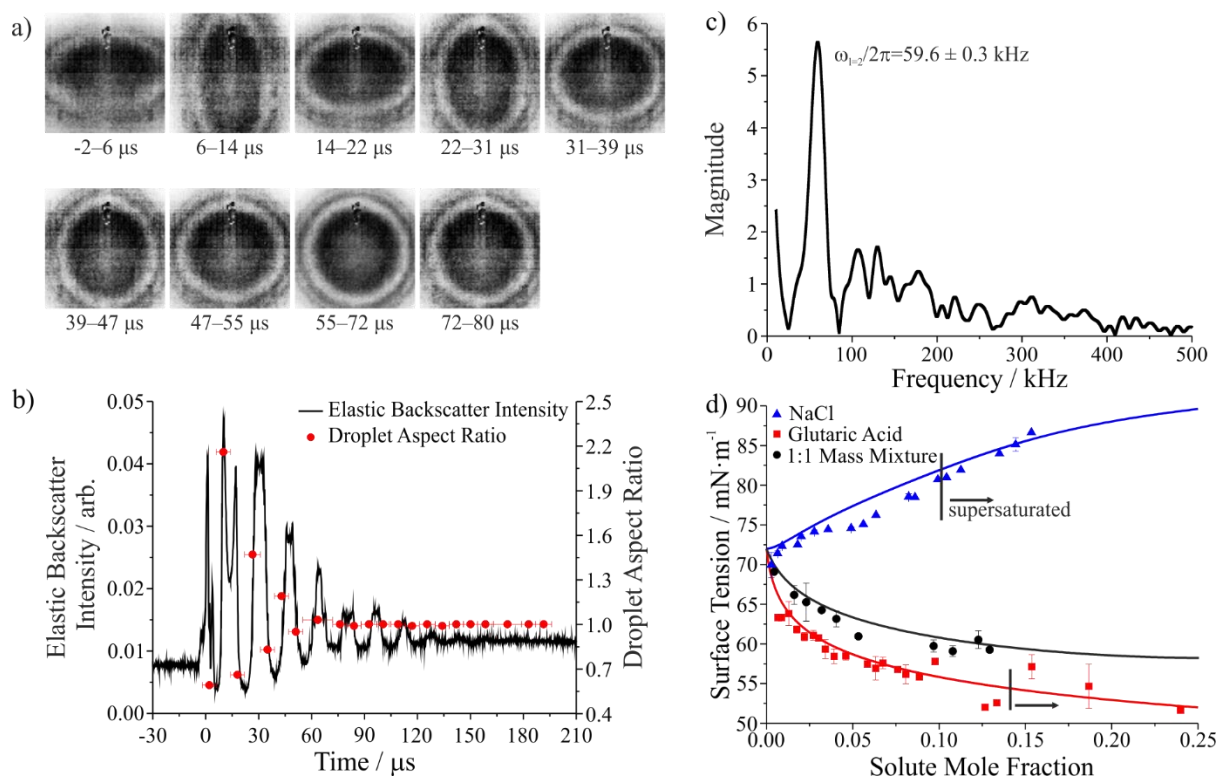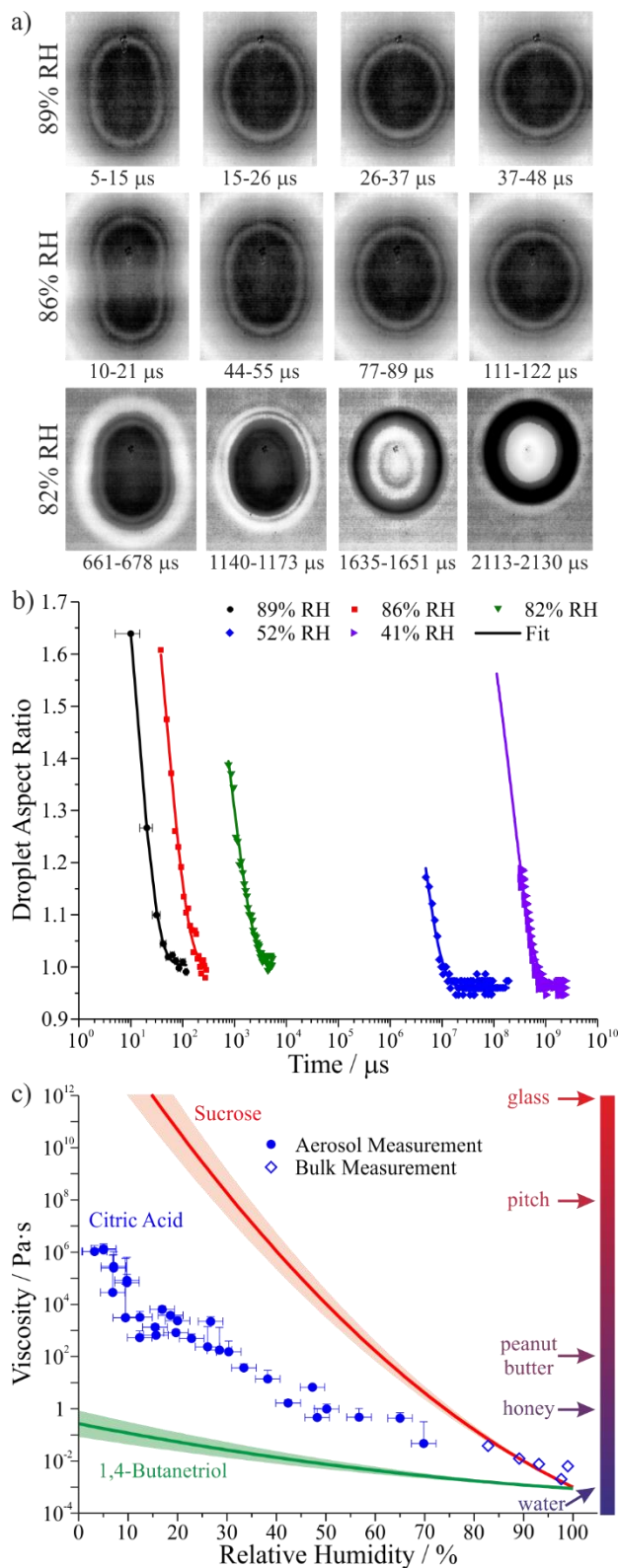
Figure 6: a) High frame rate images after coalescence of two aqueous, surfactant-doped NaCl droplets. b) Elastic backscattered light intensity collected after coalescence (left axis) and droplet aspect ratios from the images in part a) (right axis). c) A Fast Fourier Transform of the signal in part b) gives the frequency of the shape oscillations.[8] d) Measurements of picolitre droplet surface tension for NaCl, glutaric acid, and a 1:1 mass mixture of the two compounds (symbols) compared to a statistical thermodynamic model of surface tension (lines).[27]

Figure 7: a) High frame rate images of coalescing sucrose droplets equilibrated to different RH values.[29] b) Droplet aspect ratios during coalescence for several droplets, each with different viscosities.[28] c) Plot of viscosity against RH for 1,4-butanetriol, citric acid, and sucrose.
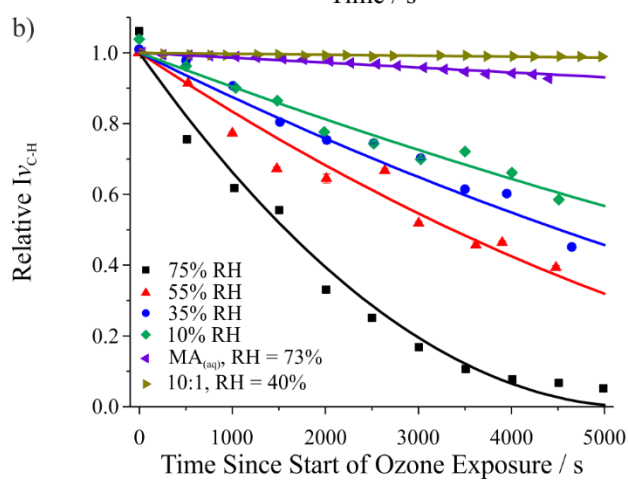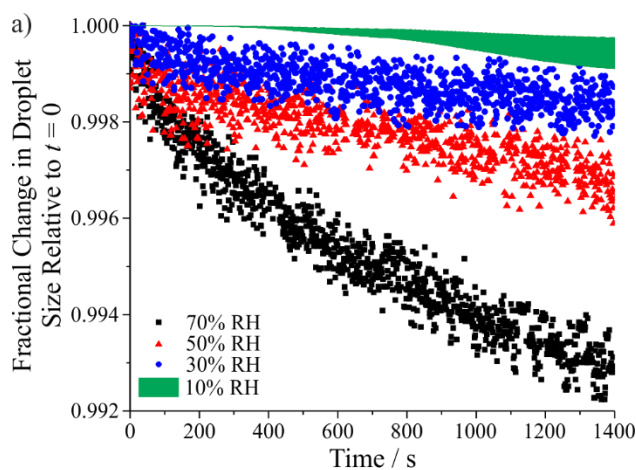
Figure 8: a) Fractional change in droplet size over 1400 s for a maleic acid-sucrose droplet at four different RH values, showing the gradual retardation in maleic acid evaporation as RH decreases. The green envelope shows the range of the data for the mixture at 10% RH (data not shown for clarity). b) Time-dependence of the normalised spontaneous Raman signal intensity of the maleic acid vinylic C-H stretch during oxidation experiments at different RH values for a 5:1 mass ratio sucrose-maleic acid. Purple triangles show change in signal intensity for an aqueous droplet evaporating at 73% RH without reaction. Gold triangles show the change in Raman intensity during reaction of a 10:1 mass ratio droplet at 40% RH.[30]